# Research on a Well-Type BGO Detector for High-Flux $\gamma$-Ray Beam Monitoring

**Ding Jiawen[1,2], Liu Longxiang[3], Wang Hongwei[2,3], Fan Gontao[2,3], Xu Hanghua[2,3], Zhang Yue[3], Chen Kaijie[5], Sun Qiankun[1,2], Hao Zirui[3], Yang Yuxuan[3], Wang Zhengwei[1,2], Xu Mengke[1,2], Zhou Mengdie[4], Wang Xiangfei[1,2]**

[1] Shanghai Institute of Applied Physics, Shanghai,201800
[2] The University of Chinese Academy of Sciences, Beijing 101408
[3] Shanghai Advanced Research Institute, Shanghai 201210
[4] School of Physics, Henan Normal University, Xinxiang 453007, China
[5] ShanghaiTech University, Shanghai, 201210, China

liulx@sari.ac.cn, wanghw@sari.ac.cn



**Abstract**

High-flux, high-energy $\gamma$-ray measurements are constrained by pulse pile-up and detector saturation. To address this issue, a well-type BGO scintillation detector based on a controlled low-efficiency sampling strategy is proposed, enabling online measurement of high-flux $\gamma$-ray beams. The design reduces the probability of full-energy absorption while maintaining a stable detector response, allowing reliable operation at elevated flux levels. The detector performance was systematically evaluated through Monte Carlo simulations, energy calibration using (p,$\gamma$) reactions, and on-beam tests at SLEGS. The results show that the detector operates stably over an energy range of 5.5–21.7 MeV at fluxes of approximately $10^5$ s$^{-1}$, without performance degradation. The experimental results agree well with the simulated one over the energy range, validating the reliability of both the model and the measured data. The detector provides an effective and scalable solution for real-time monitoring of high-flux $\gamma$-ray beams.

**Keywords -**

**BGO scintillator detector; High-flux $\gamma$-ray beam; Geant4 simulation; Well-Type**

## 1 Introduction

High-flux gamma-ray beams with tunable energy are widely used in nuclear physics, astrophysics, detector calibration, and radiation applications[1]. Recent developments in Laser Compton Scattering (LCS) sources have enabled the production of $\gamma$-ray beams with high intensity, narrow energy spread, and adjustable energy, as represented by facilities such as HI$\gamma$S(USA) [2, 3], NewSUBARU BL01 (Japan) [4, 5], ELI-NP (Europe) [6, 7], VIGAS (China) [8] and SLEGS (China)[9, 10, 11]. These advances impose stringent requirements on beam diagnostics, particularly for accurate measurements of energy spectrum and intensity.

Traditional detectors exhibit severe performance degradation under high-flux conditions, including signal saturation, pulse pile-up, and dead-time effects. These effects distort the measured energy spectra and count rate, and cannot be fully compensated by optimized readout electronics. Commonly used gamma detectors, such as NaI(Tl), BGO [12], $LaBr_3$ [13] scintillator and HPGe crystal, operate reliably at moderate count rates, but rapidly saturate at high flux due to their high intrinsic efficiency . To address these issues, several approaches have been developed, including passive attenuation with thin absorbers, detection of scattered gamma rays [14, 7], activation-based offline measurement [15, 16]and online measurement based on D($\gamma$, p)n photoneutron reactions [17]. However, these methods introduce significant distortion of the incident energy spectrum, complex background, increase the uncertainty in spectrum reconstruction, or fail to enable real-time online measurements of the energy spectrum and flux.

Based on the core concept of controlled low-efficiency sampling measurement, this paper develops a novel Well-type BGO detector(WBGO) suitable for high-flux $\gamma$-ray conditions. It is designed to achieve direct measurements of the $\gamma$-ray energy spectrum and flux in high-flux $\gamma$-ray experimental environments, avoid detector signal saturation and pulse pile-up, while minimizing interference with the primary beam.

## 2 Detector Design

Instead of pursuing high detection efficiency, a controllable low-efficiency sampling detection strategy is specifically designed for high-flux $\gamma$-ray beam environments, enabling a deliberately reduced detection efficiency tailored for such conditions. The approach relies on the interplay between interaction physics (Compton scattering and electron–positron pair production) and geometrical acceptance control. By restricting the solid-angle acceptance of scattered photons and secondary electrons through geometrical design, signal pile-up and detector saturation are effectively suppressed, thereby ensuring stable and reliable measurements.

A schematic diagram of the proposed WBGO is shown in Fig. 1. The detector is based on a cylindrical BGO crystal, identical in size to WBGO: 76.2 mm diameter and 100 mm length, with a 10 mm-diameter central borehole. A thin aluminum scattering foil with a thickness of 15 $\mu$m is positioned at the entrance of the channel. Under the thin-target condition(i.e., interaction probability $\ll 1$), the probabilities of Compton scattering and electron–positron pair production in the foil remain intrinsically low. Consequently, most incident $\gamma$ rays pass directly through the central borehole without interaction. For the small fraction of particles that undergo interactions, only a limited amount of energy is deposited in the foil, and the process is primarily manifested as angular deflection. These deflected particles subsequently enter the surrounding BGO crystal, where they deposit energy and generate scintillation signals. The rear end of the BGO crystal is optically coupled to a size-matched SiPM for scintillation light readout. The SiPM output is processed by front-end electronics and digitized by the data acquisition (DAQ) system.

The detector assembly is enclosed in a thick aluminum alloy housing for mechanical support and radiation shielding. All cylindrical components are aligned along the Z axis, forming a compact and axisymmetric configuration. Detailed detector parameters are summarized in Table 1.

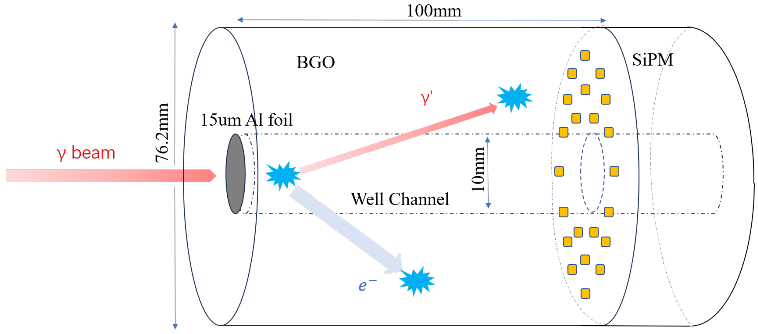


Figure 1. Schematic Diagram of the Well-Type BGO Detector

Table 1. Main parameters of the WBGO

| Parameter | Value |
|---|---|
| Diameter of WBGO | 76.2 mm |
| Length of WBGO | 100 mm |
| Thickness of SiPM | 40 mm |
| Thickness of optical coupling medium | 50 $\mu$m |
| Thickness of aluminum foil | 15 $\mu$m |
| Diameter of Well Channel | 10 mm |
| Thickness of aluminum alloy shell | 2 mm |

## 3 Experimental Setup

SLEGS is a nuclear physics beamline at SSRF that produces quasi-monoenergetic $\gamma$ rays beams via LCS mode [18]. The main components of SLEGS responsible for $\gamma$-ray generation include the interaction chamber, the multifunction chamber, and a $CO_2$ laser system. In the multifunction chamber, head-on (180°) laser–electron collisions produce backscattered $\gamma$ rays with an maximum energy of 21.7 MeV. In slant scattering mode,$\gamma$-ray energies ranging from 0.66 to 21.1 MeV can be achieved by varying the laser–electron collision angle from 20° to 160°. Therefore, the $\gamma$-ray energy can be continuously tuned by adjusting the collision angle. The SLEGS beamline employs a two-stage collimation system to control the beam spot size and energy spread, consisting of an upstream rotating lead Coarse(C) collimator with multiple apertures and a downstream Lead Three-hole(T) collimator for 1,2,3 mm aperture adjustment and beam shaping[10, 12]. The 20 mm Coarse and 2 mm Three-hole collimation(C20T2) mode was adopted in this work.

During the experiment, the WBGO was operated inside a vacuum chamber with a pressure of approximately 65 Pa to minimize additional $\gamma$-rays interactions in air. A lead collimator with an aperture matched to the detector bore was placed in front of the detector to suppress background $\gamma$-rays from off-axis directions, thereby constraining the spatial distribution of incident particles, as illustrated in Fig. 2.To ensure precise alignment of the $\gamma$-ray beam with the central bore of the WBGO, a MiniPIX pixel detector was temporarily installed downstream of the beamline to measure the transverse beam spot distribution. After alignment optimization, the MiniPIX detector was removed.

In addition, a downstream large size BGO detector (LBGO, Dia.76.2mm x Len.200 mm) was used to measure the $\gamma$-ray energy spectrum and beam flux. To avoid saturation under high-flux irradiation, a copper attenuator was placed in front of the LBGO to reduce the incident flux. Owing to the intentionally low detection efficiency of the WBGO, its interaction probability with $\gamma$ rays is extremely small, and its perturbation to the beam can be considered negligible. Therefore, the spectrum measured by the LBGO can be regarded as effectively unperturbed by the upstream detector. The measured spectra were corrected using the detector response function and subsequently unfolded to reconstruct the true incident $\gamma$-ray energy distribution [12].

Data acquisition was performed using a CAEN V1725S digitizer within the CoMPASS framework, recording three signal channels: the laser bunch signal, the WBGO signal, and the LBGO signal [19]. The laser bunch signal was used to subtract the gamma-ray background.

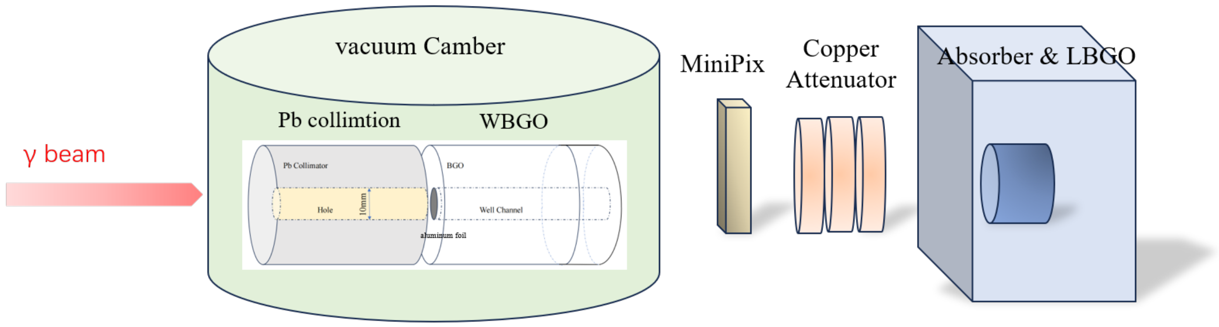


Figure 2. Layout Diagram of the SLEGS Experimental Station.

## 4 Response Simulation

To quantitatively characterize the response of the WBGO under high-flux $\gamma$-ray irradiation, a comprehensive Monte Carlo simulation framework based on Geant4 was developed, incorporating detailed detector geometry and relevant physical processes [20]. The G4EmStandardPhysics package was employed to simulate $\gamma$-ray interactions in the Aluminum foil and detector materials (e.g., Compton scattering and electron–positron pair production), while G4OpticalPhysics was used to describe scintillation photon generation and optical photon transport [21]. In contrast to conventional approaches based on empirical energy broadening, the present work implements a full-chain simulation from energy deposition to scintillation emission and subsequent optical photon transport.

A realistic optical transport model consistent with the actual detector configuration was established. This model includes scintillation photon production in the BGO crystal, photon propagation, and optical processes at material interfaces, such as reflection, refraction, and scattering. The interfaces between the crystal, reflective layers, air gaps, optical coupling media, and the SiPM were carefully modeled with appropriate optical parameters. Optical photons reaching the sensitive area of the SiPM were probabilistically converted into photoelectrons according to the photon detection efficiency (PDE), enabling a physics-based description of the detector response. Based on the statistical nature of photon detection, a response model linking deposited energy to output signal was established, with key parameters summarized in Table 2.

To ensure consistency between experimental and simulation, the $\gamma$-ray energy spectrum obtained from the LBGO via unfolding was used as the input for the simulation. The developed framework provides reliable theoretical and technical support for response function construction and incident $\gamma$-ray spectrum reconstruction of the WBGO.

Table 2. Scintillator parameters used for Geant4 simulation

| Parameter | Value |
|---|---|
| Scintillator | BGO |
| Density | 7.13 g/cm$^3$ |
| Light yield | 8500 photons/MeV |
| Emission peak | ~480 nm |
| Refractive index (BGO) | 2.11–1.32 (wavelength dependent) |
| Reflectivity (PTFE) | ~0.95 (diffuse) |
| Refractive index (coupling) | ~1.43 |
| SiPM PDE peak | ~0.49 @ 450 nm |
| PDE wavelength range | ~200–950 nm |

# 5 Experimental Results and Analysis

## 5.1 Detector validation with $^{60}$Co source

To validate the accuracy of the detector response model, measurements were performed using a standard $^{60}$Co $\gamma$-ray source and compared with Geant4 simulations. The $^{60}$Co source emits two well-defined $\gamma$ rays at 1173 keV and 1332 keV, providing a reliable probe of the detector response in the low-energy region. As shown in Fig.3(a), the comparison shows that the simulated spectra are in good agreement with the experimental data in terms of peak position, energy resolution (FWHM), and Compton continuum. This agreement indicates that the Geant4 model accurately reproduces the physical response of the detector,validating its applicability for subsequent high-energy calibration and spectral analysis.

Furthermore, without introducing any empirical energy broadening, the simulation still reproduces the measured spectral features with good accuracy, demonstrating the effectiveness of the physics-based modeling approach.

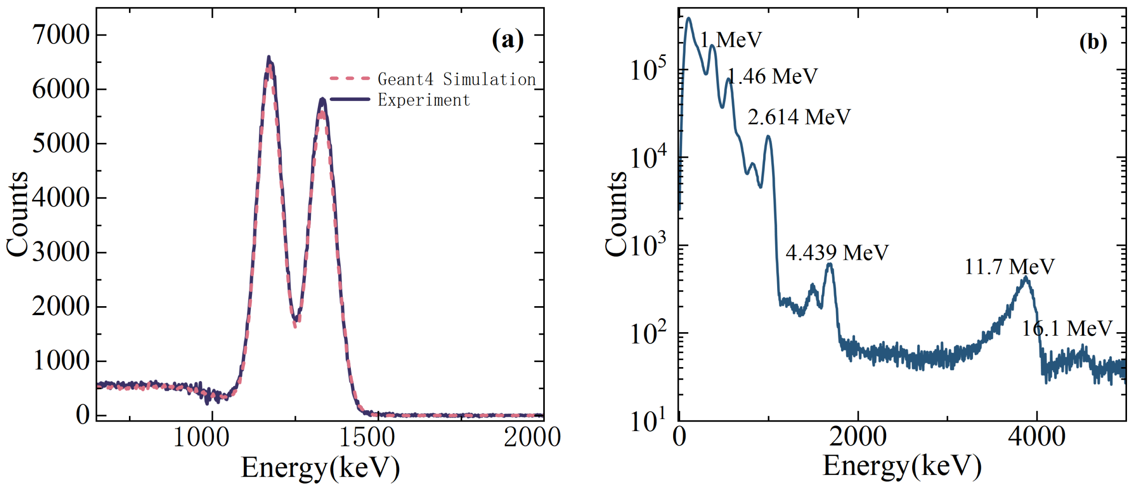


Figure 3. (a) Experimental and Geant4-simulated spectra for $^{60}$Co source. (b) Monoenergetic $\gamma$-ray spectra measured in $^{11}$B(p,$\gamma$)$^{12}$C reaction with natural radioactive background at IMP.

## 5.2 Energy response and calibration

Following model validation, a systematic study of the detector energy response was carried out using monoenergetic $\gamma$-ray calibration data from the Institute of Modern Physics (IMP, Chinese Academy of Sciences), and multi-angle measurements from the SLEGS beamline. In the IMP experiment, monoenergetic $\gamma$ rays were produced via the

$^{11}B(p,\gamma)^{12}C$ reaction, providing reference energies at 4.439, 11.7, and 16.1 MeV [22]. The corresponding spectra are shown in Fig. 3(b).

The WBGO detector exhibits a low-energy background, primarily originating from intrinsic radioactivity of the crystal, trace radioactive impurities, and environmental radiation. In particular, $\alpha$-emitting isotopes such as $^{210}Po$, produced via neutron activation of bismuth, contribute significantly to the low-energy region due to the reduced light yield of WBGO for $\alpha$ particles[23]. In addition, natural radioactive decay chains and ambient $\gamma$ radiation form a continuous background component.

Based on these data, the monoenergetic $\gamma$ rays from the IMP experiment (4.439, 11.7, and 16.1 MeV) were used as primary calibration reference points, while characteristic low-energy background features (e.g., $^{40}K$ and $^{232}Th$) provided auxiliary constraints on the detector response in the low-energy region. This enabled the establishment of a quantitative relationship between the detector output ( in ADC Channel) and the incident $\gamma$-ray energy. To extend the calibration to higher energies, SLEGS multi-angle data were incorporated, with $\gamma$-ray energies independently determined by the beam monitoring system. The resulting energy response and corresponding fitting results as shown in Fig.4.

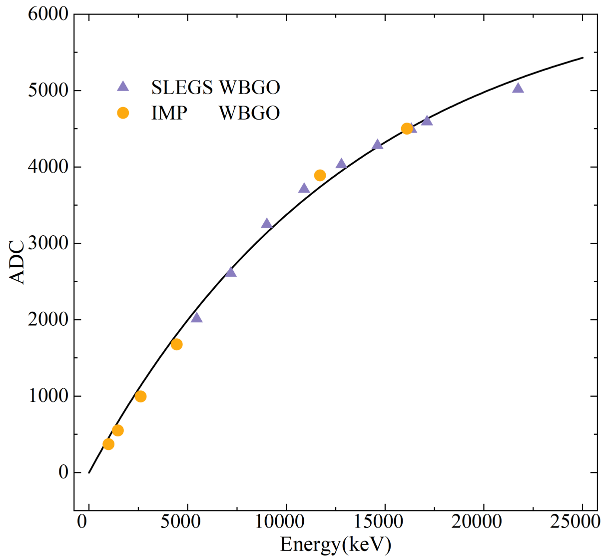


Figure 4. Detector energy response with IMP and SLEGS data; the curve shows the nonlinear fit based on the SiPM saturation model.

Due to the finite number of microcells in silicon photomultipliers (SiPMs), saturation effects arise under high photon flux, leading to a nonlinear detector response. To account for this behavior, a microcell-based saturation model, which is widely used to describe SiPM saturation under high photon flux conditions, was employed to characterize the detector response[24, 25, 26]. The saturation model is given by the following equation:

$$N_{\text{fired}} = N_{\text{total}} \times \left\{ 1 - \exp\left( \frac{-N_{\text{photon}} \times \text{PDE}}{N_{\text{total}}} \right) \right\}, \tag{1}$$

where $N_{\text{fired}}$, $N_{\text{total}}$, $N_{\text{photon}}$ and PDE denote the number of fired pixels (corresponding to the actual output signal of the detector, e.g., the ADC channel), total number of microcells, number of scintillation photons incident on the SiPM, and photon detection efficiency, respectively.

Fitting the experimental data yields an effective number of microcells $N_{\text{total}} = 6429.33$ and an effective photon detection efficiency PDE = 0.479. Here, $N_{\text{total}}$ represents the effective number of pixels, while PDE is an effective parameter incorporating both intrinsic detection efficiency and optical collection efficiency.

The inverse form of this model was subsequently constructed to correct for the nonlinear response, enabling the conversion from detector output to incident $\gamma$-ray energy. Using the calibrated response function, the peak positions measured at SLEGS were converted into reconstructed $\gamma$-ray energies $E_{\text{rec}}$,which were then compared with the reference energies $E_{\text{monitor}}$ provided by the beam monitoring system. The relative deviation is defined as:

$$D_E = \frac{E_{\text{rec}} - E_{\text{monitor}}}{E_{\text{monitor}}}. \tag{2}$$

The average deviation is 3.7% over the entire investigated energy range, demonstrating good consistency of the response model. The remaining discrepancies are attributed to uncertainties in energy calibration, beam energy determination, and statistical fluctuations in the measured spectra. At the highest energy point (corresponding to 180° backscattering), the deviation increases slightly. This behavior is attributed to enhanced nonlinearity effects in the SiPM response and increased sensitivity to model parameters under high photon flux conditions.

## 6 Results of SLEGS Online Experiment

Figure 5 presents the online experimental results obtained at the SLEGS beamline. During the measurements, eight energy points were selected under an oblique incidence configuration, together with additional points in the backscattering mode, where both the WBGO and the beam monitoring system were operated simultaneously. The background-subtracted spectra measured by the WBGO were compared with Geant4 simulation results. The incident $\gamma$-ray energy distribution used in the simulation was obtained by unfolding the spectrum measured with the LBGO.

The results show that the background-subtracted experimental spectra are in excellent agreement with the simulated spectra over the investigated energy range. This agreement validates that the combination of the WBGO design, accurate energy calibration, background subtraction, spectrum unfolding from the LBGO, and the Geant4 response model enables a consistent and quantitative reconstruction of $\gamma$-ray spectra at different incident angles. Minor discrepancies observed in the low-energy region are mainly attributed to limitations in the detector modeling and input assumptions, including electronic noise, baseline fluctuations, and possible nonlinear effects in scintillation light yield and SiPM response. In addition, the online background is mainly caused by incomplete suppression of scattered $\gamma$ rays in air and near the entrance of the beamline by the lead collimator.

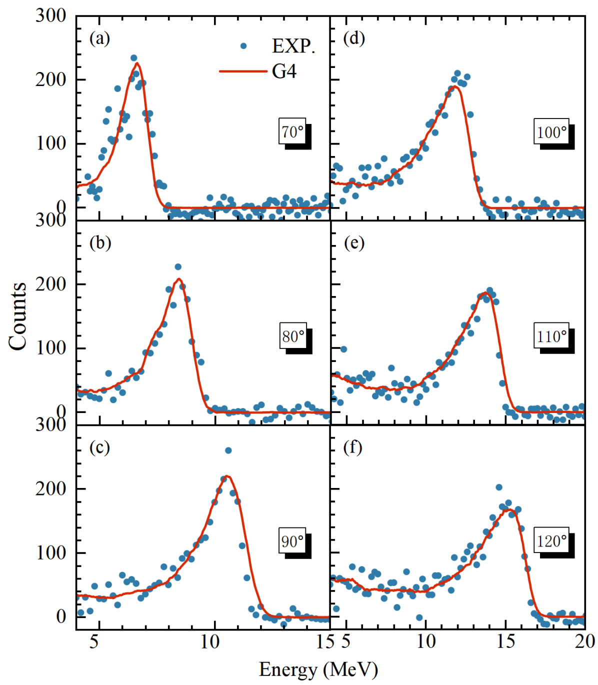


Figure 5. Comparison of online-measured laser gamma spectra (online background subtracted) and simulation using a well-type BGO detector.

Figure 6 shows the detection efficiency of the WBGO detector as a function of $\gamma$-ray energy. The experimental results demonstrate that the detection efficiency remains at the level of $10^{-5}$ over the full energy range, decreasing monotonically from approximately $8.6\times10^{-5}$ at 5.5 MeV to approximately $5.7\times10^{-5}$ at 21.7 MeV. This controlled low efficiency is a direct consequence of the sampling strategy, enabling stable operation under high-flux $\gamma$-ray conditions.

The Geant4 simulation results are in good agreement with the experimental data across the entire angular range. To quantitatively evaluate the agreement, the relative deviation is defined as: $(\varepsilon_{\text{sim}}-\varepsilon_{\text{exp}})/\varepsilon_{\text{exp}}$, is shown in the lower panel of Fig.6. where $\varepsilon_{\text{sim}}$ and $\varepsilon_{\text{exp}}$ denote the simulated and experimental efficiencies,respectively. The deviation remains within 2.3% for all angles, indicating that the simulation reproduces the measured efficiency with high accuracy. A slightly larger deviation is observed in the intermediate angular range (approximately 12.8 MeV–16.3 MeV),which can be attributed to experimental uncertainties and approximations in the simulation.

Overall, the simulation results are consistent with the experimentally observed efficiency and its angular dependence, further validating the proposed low-efficiency sampling detection approach.

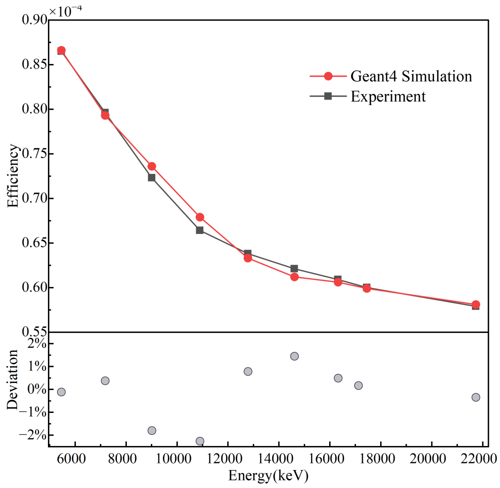


Figure 6. Detection efficiency of the well-type BGO detector as a function of energy. The upper panel shows the comparison between experimental data and Geant4 simulation, while the lower panel presents the relative difference $(\varepsilon_{\text{sim}}-\varepsilon_{\text{exp}})/\varepsilon_{\text{exp}}$.

## 7 Summary

A well-type BGO detector for high-flux $\gamma$-ray beam monitoring has been developed based on a controlled low-efficiency sampling strategy. By combining a central bore structure with an ultrathin aluminum scatterer, the detection efficiency is maintained at the level of $10^{-5}$, allowing most incident $\gamma$ rays to pass through without interaction. This design effectively suppresses pulse pile-up and saturation while preserving sensitivity to beam characteristics. A comprehensive Geant4-based response model, incorporating $\gamma$-ray interactions, energy deposition, and optical photon transport, was established. Together with monoenergetic $\gamma$-ray data from IMP and multi-angle measurements from SLEGS, a nonlinear energy calibration method accounting for SiPM saturation was developed. The reconstructed energies agree with independently measured beam energies with an average deviation of 3.7% over most of the energy range. Good agreement between background-subtracted experimental spectra and simulations further demonstrates the self-consistency of the response model and analysis framework. In addition, the detection efficiency agrees well with simulations over the full angular range, with relative deviations below 2.3%.

To explore the applicability at even higher flux levels, a preliminary Geant4-based study of key structural parameters was performed. The results show that reducing the thickness of the aluminum foil or enlarging the central bore can further decrease the interaction probability. These results indicate that a flexible balance between detection efficiency and linear response range can be achieved through parameter optimization.

Overall, the proposed detector demonstrates stable and controllable performance under ultra-low-efficiency conditions, providing an effective and scalable solution for high-flux $\gamma$-ray beam diagnostics and spectroscopy.

## References


[1] Dmitry Budker, Julian C. Berengut, Victor V. Flambaum, Mikhail Gorchtein, Junlan Jin, Felix Karbstein, Mieczyslaw Witold Krasny, Yuri A. Litvinov, Adriana Pálffy, Vladimir Pascalutsa, Alexey Petrenko, Andrey Surzhykov, Peter G. Thirolf, Marc Vanderhaeghen, Hans A. Weidenmüller, and Vladimir Zelevinsky. Expanding nuclear physics horizons with the gamma factory. *Annalen der Physik*, 534(3):2100284, 2022. doi:https://doi.org/10.1002/andp.202100284. URL `https://onlinelibrary.wiley.com/doi/abs/10.1002/andp.202100284`.

[2] Henry R. Weller, MohammadW. Ahmed, and Ying Wu. Nuclear physics research at the high intensity gamma-ray source (HI$\gamma$S). *Nuclear Physics News*, 25:19 – 24, 2015. URL `https://api.semanticscholar.org/CorpusID:120009084`.

[3] V. N. Litvinenko, B. Burnham, M. Emamian, N. Hower, J. M. J. Madey, P. Morcombe, P. G. O'Shea, S. H. Park, R. Sachtschale, K. D. Straub, G. Swift, P. Wang, Y. Wu, R. S. Canon, C. R. Howell, N. R. Roberson, E. C. Schreiber, M. Spraker, W. Tornow, H. R. Weller, I. V. Pinayev, N. G. Gavrilov, M. G. Fedotov, G. N. Kulipanov, G. Y. Kurkin, S. F. Mikhailov, V. M. Popik, A. N. Skrinsky, N. A. Vinokurov, B. E. Norum, A. Lumpkin, and B. Yang. Gamma-ray production in a storage ring free-electron laser. *Phys. Rev. Lett.*, 78:4569–4572, Jun 1997. doi:10.1103/PhysRevLett.78.4569. URL `https://link.aps.org/doi/10.1103/PhysRevLett.78.4569`.

[4] Sho Amano, Ken Horikawa, Kazuki Ishihara, Shuji Miyamoto, Takehito Hayakawa, Toshiyuki Shizuma, and Takayasu Mochizuki. Several-mev $\gamma$-ray generation at NewSUBARU by laser compton backscattering. *Nuclear Instruments and Methods in Physics Research Section A: Accelerators, Spectrometers, Detectors and Associated Equipment*, 602(2):337–341, 2009. ISSN 0168-9002. doi:https://doi.org/10.1016/j.nima.2009.01.010. URL `https://www.sciencedirect.com/science/article/pii/S0168900209000278`.

[5] Ken Horikawa, Shuji Miyamoto, Sho Amano, and Takayasu Mochizuki. Measurements for the energy and flux of laser compton scattering $\gamma$-ray photons generated in an electron storage ring: Newsubaru. *Nuclear Instruments and Methods in Physics Research Section A: Accelerators, Spectrometers, Detectors and Associated Equipment*, 618(1):209–215, 2010. ISSN 0168-9002. doi:https://doi.org/10.1016/j.nima.2010.02.259. URL `https://www.sciencedirect.com/science/article/pii/S0168900210005449`.

[6] A. Zilges, D.L. Balabanski, J. Isaak, and N. Pietralla. Photonuclear reactions—from basic research to applications. *Progress in Particle and Nuclear Physics*, 122:103903, 2022. ISSN 0146-6410. doi:https://doi.org/10.1016/j.ppnp.2021.103903. URL `https://www.sciencedirect.com/science/article/pii/S0146641021000624`.

[7] G.V. Turturica, C. Matei, A. Pappalardo, D.L. Balabanski, S. Chesnevskaya, V. Iancu, C.A. Ur, H.J. Karwowski, K.A. Chipps, M.T. Febbraro, S.D. Pain, D. Walter, C.Aa. Diget, J. Frost-Schenk, M. Munch, G.L. Guardo, M. La Cognata, R.G. Pizzone, G.G. Rapisarda, K.Y. Chae, M.J. Kim, and M.S. Kwag. Investigation of compton scattering for gamma beam intensity measurements and perspectives at ELI-NP. *Nuclear Instruments and Methods in Physics Research Section A: Accelerators, Spectrometers, Detectors and Associated Equipment*, 921:27–32, 2019. ISSN 0168-9002. doi:https://doi.org/10.1016/j.nima.2018.12.048. URL `https://www.sciencedirect.com/science/article/pii/S016890021831845X`.

[8] Xian-Cai Lin, Hao Zha, Jia-Ru Shi, Qiang Gao, Jia-Yang Liu, Liu-Yuan Zhou, Jian Gao, Huai-Bi Chen, and Chuan-Xiang Tang. Fabrication, tuning, and high-gradient testing of an x-band traveling-wave accelerating structure for VIGAS. *Nuclear Science and Techniques*, 33(8):102, August 2022. ISSN 2210-3147. doi:10.1007/s41365-022-01086-y. URL `https://doi.org/10.1007/s41365-022-01086-y`.

[9] Long-Xiang Liu, Hong-Wei Wang, Gong-Tao Fan, Hang-Hua Xu, Yue Zhang, Zi-Rui Hao, and Ai-Guo Li. The SLEGS beamline of SSRF. *Nuclear Science and Techniques*, 35:2210–3147, 2024. ISSN 7. doi:10.1007/s41365-024-01469-3. URL `https://doi.org/10.1007/s41365-024-01469-3`.

[10] Hong-Wei Wang, Gong-Tao Fan, Long-Xiang Liu, Hang-Hua Xu, Wen-Qing Shen, Yu-Gang Ma, Hiroaki Utsunomiya, Long-Long Song, Xi-Guang Cao, Zi-Rui Hao, Kai-Jie Chen, Sheng Jin, Yu-Xuan Yang, Xin-Rong Hu, Xin-Xiang Li, and Pan Kuang. Commissioning of laser electron gamma beamline slegs at ssrf.

*Nuclear Science and Techniques*, 33:2210–3147, 2022. ISSN 7. doi:10.1007/s41365-022-01076-0. URL https://doi.org/10.1007/s41365-022-01076-0.

[11] H.H. Xu, G.T. Fan, H.W. Wang, H. Utsunomiya, L.X. Liu, Z.R. Hao, H.L. Wu, L.L. Song, Q.L. Zhang, B.C. Jiang, X.R. Hu, X.X. Li, P. Kuang, Y.X. Yang, and S. Jin. Interaction chamber for laser Compton slant-scattering in SLEGS beamline at Shanghai Light Source. *Nuclear Instruments and Methods in Physics Research Section A: Accelerators, Spectrometers, Detectors and Associated Equipment*, 1033:166742, 2022. ISSN 0168-9002. doi:https://doi.org/10.1016/j.nima.2022.166742. URL https://www.sciencedirect.com/science/article/pii/S0168900222002625.

[12] L.X. Liu, H. Utsunomiya, G.T. Fan, H.H. Xu, H.W. Wang, Z.R. Hao, Y. Zhang, C.Y. He, P. Jiao, S. Ye, S. Jin, K.J. Chen, Y.X. Yang, Q.K. Sun, Z.W. Wang, Z.C. Li, M.D. Zhou, X. Lu, C. Yang, F. Lu, and X.G. Cao. Energy profile of laser Compton slant-scattering $\gamma$-ray beams determined by direct unfolding of total-energy responses of a BGO detector. *Nuclear Instruments and Methods in Physics Research Section A: Accelerators, Spectrometers, Detectors and Associated Equipment*, 1063:169314, 2024. ISSN 0168-9002. doi:https://doi.org/10.1016/j.nima.2024.169314. URL https://www.sciencedirect.com/science/article/pii/S0168900224002407.

[13] Longxiang Liu, Yue Zhang, Zirui Hao, Gongtao Fan, Hongwei Wang, Hanghua Xu, Chuangye He, Pu Jiao, Shan Ye, Yuxuan Yang, Sheng Jin, Kaijie Chen, Zhicai Li, Qiankun Sun, Zhenwei Wang, Mengke Xu, Xiangfei Wang, Mengdie Zhou, Yulong Shen, and Chang Yang. Direct unfolding determination of energy spectra using a $LaBr_3$ detector for SLEGS. *Nuclear Instruments and Methods in Physics Research Section A: Accelerators, Spectrometers, Detectors and Associated Equipment*, 1083:171075, 2026. ISSN 0168-9002. doi:https://doi.org/10.1016/j.nima.2025.171075. URL https://www.sciencedirect.com/science/article/pii/S0168900225008770.

[14] Xuanqi Zhang, Yulan Li, Zhi Zhang, Yang Tian, Zhijun Chi, Hao Ding, Hongze Zhang, Jin Lin, Yingchao Du, and Chuanxiang Tang. A compton scattering-based energy spectrum measurement method for high flux gamma-ray of VIGAS facility. *Nuclear Instruments and Methods in Physics Research Section A: Accelerators, Spectrometers, Detectors and Associated Equipment*, 1085:171278, 2026. ISSN 0168-9002. doi:https://doi.org/10.1016/j.nima.2026.171278. URL https://www.sciencedirect.com/science/article/pii/S0168900226000045.

[15] R.E. Pywell, O. Mavrichi, W.A. Wurtz, and R. Wilson. Photon flux monitor for a mono-energetic gamma ray source. *Nuclear Instruments and Methods in Physics Research Section A: Accelerators, Spectrometers, Detectors and Associated Equipment*, 606(3):517–522, 2009. ISSN 0168-9002. doi:https://doi.org/10.1016/j.nima.2009.04.014. URL https://www.sciencedirect.com/science/article/pii/S0168900209007876.

[16] Yu-Xuan Yang, Yue Zhang, Zhi-Cai Li, Zi-Rui Hao, Sheng Jin, Kai-Jie Chen, Zhen-Wei Wang, Qian-Kun Sun, Gong-Tao Fan, Hang-Hua Xu, Long-Xiang Liu, Wei-Juan Zhao, and Hong-Wei Wang. Beam flux measurement using a photon activation analysis method at the SLEGS. *Nuclear Science and Techniques*, 36(5):73–80, May 2025.

[17] C. Matei, J.M. Mueller, M.H. Sikora, G. Suliman, C.A. Ur, and H.R. Weller. Investigation of the d($\gamma$,n)p reaction for gamma beam monitoring at ELI-NP. *Journal of Instrumentation*, 11(05):P05025, may 2016. doi:10.1088/1748-0221/11/05/P05025. URL https://doi.org/10.1088/1748-0221/11/05/P05025.

[18] Ren Zhong Tai and Zhen Tang Zhao. Overview of SSRF phase-II beamlines. *Nuclear Science and Techniques*, 35:137, 2024. doi:10.1007/s41365-024-01487-1.

[19] CAEN. Caen-tools for discovery. URL https://www.caen.it/. 2023.

[20] S. Agostinelli, J. Allison, K. Amako, and J. Apostolakis. Geant4—a simulation toolkit. *Nuclear Instruments and Methods in Physics Research Section A: Accelerators, Spectrometers, Detectors and Associated Equipment*, 506(3):250–303, 2003. ISSN 0168-9002. doi:https://doi.org/10.1016/S0168-9002(03)01368-8. URL https://www.sciencedirect.com/science/article/pii/S0168900203013688.

[21] A. Khodaei, A.N.Z. Rashed, F. Moradi, H.A. Abdul-Rashid, and D.A. Bradley. A review of the geant4 simulation platform for applications involving optical-based sensing and dosimetry. *Radiation Physics and Chemistry*, 212: 111062, 2023. ISSN 0969-806X. doi:https://doi.org/10.1016/j.radphyschem.2023.111062. URL https://www.sciencedirect.com/science/article/pii/S0969806X23003079.

[22] J. J. He, B. L. Jia, S. W. Xu, S. Z. Chen, S. B. Ma, S. Q. Hou, J. Hu, L. Y. Zhang, and X. Q. Yu. Direct measurement of $^{11}$B(p,$\gamma$)$^{12}$C astrophysical S factors at low energies. *Physical Review C*, 93(5), May 2016. ISSN 2469-9993. doi:10.1103/physrevc.93.055804. URL http://dx.doi.org/10.1103/PhysRevC.93.055804.

[23] D.N. Grigoriev, V.F. Kazanin, G.N. Kuznetcov, I.I. Novoselov, P. Schotanus, B.M. Shavinski, S.N. Shepelev, V.N. Shlegel, and Ya.V. Vasiliev. Alpha radioactive background in BGO crystals. *Nuclear Instruments and Methods in Physics Research Section A: Accelerators, Spectrometers, Detectors and Associated Equipment*, 623 (3):999–1001, 2010. ISSN 0168-9002. doi:https://doi.org/10.1016/j.nima.2010.07.067. URL https://www.sciencedirect.com/science/article/pii/S0168900210016815.

[24] L. Gruber, S.E. Brunner, J. Marton, and K. Suzuki. Over saturation behavior of sipms at high photon exposure. *Nuclear Instruments and Methods in Physics Research Section A: Accelerators, Spectrometers, Detectors and Associated Equipment*, 737:11–18, 2014. ISSN 0168-9002. doi:https://doi.org/10.1016/j.nima.2013.11.013. URL https://www.sciencedirect.com/science/article/pii/S0168900213015520.

[25] Q. Weitzel, P. Bernhard, A.S. Brogna, R. Degele, S. Krause, U. Schäfer, and S. Tapprogge. Measurement of the response of silicon photomultipliers from single photon detection to saturation. *Nuclear Instruments and Methods in Physics Research Section A: Accelerators, Spectrometers, Detectors and Associated Equipment*, 936:558–560, 2019. ISSN 0168-9002. doi:https://doi.org/10.1016/j.nima.2018.10.074. URL https://www.sciencedirect.com/science/article/pii/S0168900218313883. Frontier Detectors for Frontier Physics: 14th Pisa Meeting on Advanced Detectors.

[26] Emilie Roncali and Simon R. Cherry. Application of silicon photomultipliers to positron emission tomography. *Annals of Biomedical Engineering*, 39(4):1358–1377, February 2011. ISSN 1573-9686. doi:10.1007/s10439-011-0266-9. URL http://dx.doi.org/10.1007/s10439-011-0266-9.